Wiley Online Library
Early View publication on www.wileyonlinelibrary.com
(issue and page numbers not yet assigned;
citable using Digital Object Identifier – **DOI**)

Phys. Status Solidi B, 1–8 (2016) / **DOI** 10.1002/pssb.201600333

physica status solidi b
www.pss-b.com
basic solid state physics

Electrodeposited *n*-type cuprous oxide cubic nanostructures for liquefied petroleum gas sensing

J. L. K. Jayasingha[1], K. M. D. C. Jayathilaka[2], M. S. Gunewardene[1], D. P. Dissanayake[3], and J. K. D. S. Jayanetti[*,1]

[1] Department of Physics, University of Colombo, Colombo 03, Sri Lanka
[2] Department of Physics, University of Kelaniya, Kelaniya, Sri Lanka
[3] Department of Chemistry, University of Colombo, Colombo 03, Sri Lanka

Received 23 May 2016, revised 2 September 2016, accepted 2 September 2016
Published online 23 September 2016

Keywords Cu_2O, electrodeposition, gas, hydrocarbons, liquefied petroleum, nanocubes, sensing, thin films

[*] Corresponding author: e-mail sumedhajayanetti@gmail.com, Phone/Fax: +94 112584777

A surfactant free template assisted electrodeposition method was used to fabricate thick *n*-type Cu_2O films having cubic nanostructures for the detection of liquefied petroleum (LP) gas at low concentrations. Templates were fabricated by initially electrodepositing a *p*-type Cu_2O thin film on a Ti substrate followed by annealing that changed conductivity type of the film, as confirmed by Mott–Schottky and spectral response measurements. SEM measurements of resulting films showed nano-cubic crystals having sizes of 150–300 nm. When exposed to a mixture of LP gas and dry air, the resistance of these films increased and the maximum response was recorded when films were maintained at 180 °C for all concentrations and it was independent of the surface morphology. At 180 °C, at the lowest tested LP gas concentration of 2 vol.%, a twofold increase in response was observed in the nano-cubic films compared to the micro-crystalline *n*-type Cu_2O films. This improvement in gas response is attributed to increased effective surface area of these nanostructured films. Compared to other LP gas sensing materials, Cu_2O films showed very good response times and recovery times of ~120 and ~90 s, respectively.

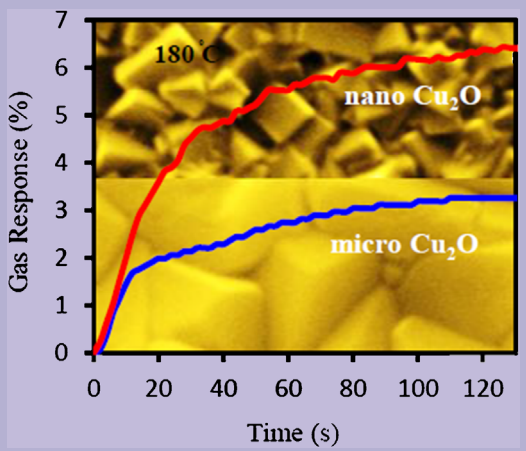

1 Introduction Cuprous oxide (Cu_2O) is a well-known metal oxide semiconductor with a direct band gap of ~2.0 eV and having a cubic crystal structure with a lattice parameter of 4.27 Å. Cu_2O is considered as an earth abundant, green material having a great potential to be used in many applications such as photovoltaics [1, 2], gas sensing [3], electro-catalysis [4, 5], and photocatalysis [6, 7]. Due to the presence of Cu vacancies in the crystal lattice, Cu_2O has been generally known as a *p*-type semiconductor [8]. However, it is now well known that Cu_2O thin films of both *p*-type and *n*-type conductivities can be grown using electrochemical deposition, a relatively simple thin film fabrication technique [1, 8, 9]. Additionally, the scalability and the ability to grow films having different surface morphologies are advantages of the electrochemical deposition [10–12]. Cu_2O thin films have been fabricated electrochemically on conducting substrates by reduction of Cu (II) in lactate [9, 13], acetate [14], or nitrate [15] baths under various deposition conditions. Deposition parameters such as bath pH, temperature, concentration of the constituent ions as well as applied electrode potential and the deposition current density across the electrodes enables

the modulation of deposited film characteristics. Among other characteristics, it has been shown that the resultant surface morphology of the thin films is highly sensitive to variation of above parameters [8]. As a semiconductor, the carrier concentration of Cu_2O is relatively low ($\sim 10^{14}$–$10^{15}\,cm^{-3}$) [3]. Therefore, from the perspective of a sensing material, to improve charge transport characteristics, adsorption capacity or photoresponse characteristics of Cu_2O thin films, modulating morphology at the nano scale has been considered important because it leads to reduced recombination of carriers [1]. Also, the high surface to volume ratio at nano scale, assists charge carrier generation through the associated physical/chemical sensing process. On the other hand, at nano scale, it is also possible to have more defect sites due to the increase in the number of grain boundaries. It is also worth noting that, controllability of the shape of the surface features also have an effect on the sensing performance. Recently, Won et al. [4] demonstrated that the electro-catalytic properties of Cu_2O and Au/Cu_2O show a dependence on the shapes of the underlying surface structures. Furthermore, it is also reported that some materials loose sensitivity due to aging of the material and due to other external factors such as humidity [16]. Therefore, for optimal sensor performance, careful optimization of surface morphology (both size and shape) and stability of fabricated material over time are important. Electrochemical deposition has been used previously to fabricate nanostructured Cu_2O thin films and has been utilized for photovoltaic applications [1, 8, 17]. Among the many sensing applications of Cu_2O (see Table 1 for a summary), microcrystalline *p*-type Cu_2O thin films fabricated using chemical bath deposition have been used for sensing of Methane [3] and NO_2 gases [18], while Cu/Cu_2O nano-crystalline hollow spheres synthesized using a micro-wave assisted hydrothermal method has shown the ability to detect NO_2 at room temperature [7]. Sensing of H_2 has been demonstrated with *p*-type Cu_2O nano-crystal films as well as Zn doped *p*-type Cu_2O films [19] and Zn-doped CuO:Zn/Cu_2O:Zn nano-scale *p*–*p* hetero-junctions [20] fabricated from chemical bath deposition method. Higher sensing response to acetone has been reported using porous micro-structured CuO/Cu_2O cubes synthesized by calcination at different temperatures [21]. It has also been reported that mono-disperse Cu_2O and CuO nano-spheres synthesized by hydrothermal process show good response in the presence of alcohol and gas oil [22]. Microcrystalline *n*-type Cu_2O thin films have been used for sensing of liquefied petroleum (LP) gas [23], a potentially hazardous yet, being used extensively for cooking or as a fuel for vehicles. Detection of LP gas at low concentrations with a fast response is thus important to ensure user safety in avoiding hazards due to accidental leak of the gas. Several metal oxide materials such as SnO_2 [24, 25], ZnO [26, 27], TiO_2 [28], CdO [16], and their sensing properties have been investigated for the purpose of LP gas sensing. Bandara et al. [23] recently reported the use of chlorine doped *n*-type Cu_2O thin films having nano-scale surface morphology with grains of arbitrary shapes. However, the literature on the use of electrodeposited Cu_2O thin film semiconductors as a LP gas sensing material has been quite limited. Furthermore, the high responses shown by TiO_2 and CdO to LP gas occur at higher temperatures while ZnO and SnO_2-based materials that have good responses even at room temperature show latency in sensing response and recovery.

The main motivation behind the present work is to demonstrate firstly, how nanostructured Cu_2O thin films with definite shapes would lead to enhanced LP gas sensing response properties without the need for doping or passivation and secondly, to show how Cu_2O nanostructures with definite shapes could be fabricated through the careful modulation of electrodeposition parameters, especially the bath pH. This is demonstrated through the fabrication of *n*-type Cu_2O thin films with nano-cubic surface morphology via a two-step electrodeposition process. Initially, a template was fabricated by electrodepositing *p*-type Cu_2O on a Ti substrate in an acetate bath followed by annealing to change the conductivity. These films having nano-cubic morphology were subsequently used to grow thicker *n*-type Cu_2O films while preserving the surface morphology, a fabrication route previously demonstrated by Jayathilaka et al. [1] to increase the photovoltaic efficiency of Ti/nano Cu_2O/Cu_xS/Au cell structures.

2 Experimental Deposition bath electrolyte was prepared by mixing of 0.1 M sodium acetate (Sigma–Aldrich, purity $\geq$99.0%), 0.01 M cupric acetate (Sigma–Aldrich, purity $\geq$99.0%), and distilled water. During electrodeposition of thin films the temperature of the electrolyte was maintained at 60 °C and stirred with a magnetic stirrer throughout the deposition. The counter electrode and the reference electrode were a platinum plate and a saturated calomel electrode (SCE) respectively. Thin film deposition was accomplished potentiostatically (Hokuto-Denko-Potentiostat/Galvanostat-HA301) at an applied potential maintained at −200 mV versus SCE. The pH of the electrolyte was adjusted by adding a diluted 2 M NaOH (Sigma–Aldrich, purity $\geq$98.0%)) solution whenever necessary. First, *p*-type nano-cubic Cu_2O thin films were deposited on Ti substrates in an acetate bath containing 0.1 M sodium acetate and 0.01 M cupric acetate by adjusting electrolyte pH to 7.6. The deposition was carried out for a duration of 30 min. Annealing the thin films at 200 °C for a duration of 5 min in air converted the conductivity of the films to *n*-type. These films were then used as templates to make thicker *n*-type Cu_2O films by electrochemical deposition in an acetate bath of pH 6.0 for a duration of 30 min [1]. Another set of films having microcrystalline surface morphological properties were fabricated on Ti substrates using an acetate bath maintained at a pH of 6.0 without using a template as described above. The deposition time was 60 min. At each stage of deposition, in order to monitor the conductivity type of the deposited films, Mott–Schottky plots were

Table 1 LP and other gas responses on Cu_2O-based and some other metal oxide-based semiconducting thin films.

morphology and properties of sensing materials	gas type	concentration	response time	recovery time	gas response/ sensitivity	temperature	ref. (year)
TiO_2 interconnected web-like structures	LPG	0.08 vol.%	165 s	240 s	35.8%	425 °C	[28] (2008)
CdO nanorods, thickness ~30–50 nm	LPG	0.2 vol.%	~110 s	~140 s	23.28%	425 °C	[16] (2008)
ZnO crystallites, size ~50 nm	LPG	4 vol.%	600 s	–	12.3	RT	[27] (2013)
ZnO nanosheets 60–200 nm	LPG	–	8 min	–	7.81 $M\Omega\,min^{-1}$	RT	[26] (2009)
SnO_2 spherical grains, minimum crystallite size ~14 nm	LPG	–	~110 s	~350 s	312%	RT	[24] (2012)
Pd doped ZnO spherical grains of ~250 nm	LPG	0.4 vol.%	15 s	–	57%	275 °C	[33] (2007)
ZnO minimum (~103 nm)	LPG	1 vol.%	–	–	~40%	325 °C	[34] (2008)
CuO:Zn/Cu_2O:Zn nano-crystallite film, diameter ~40–60 nm, thickness ~600 nm	H_2	100 ppm	~2 s	~5.5 s	~1000%	300 °C	[20] (2016)
porous CuO/Cu_2O cubes	acetone	500 nm	1 s	25 s	9.7	150 °C	[21] (2013)
n-Cu_2O microcrystalline (~1 μm)	LPG	2 vol.%	~90 s	~130 s	3.2%	180 °C	this work
n-Cu_2O nano-cubes (~150–300 nm)	LPG	2 vol.%	~120 s	~90 s	6.5%	180 °C	this work

obtained through electrochemical impedance measurements which were carried out at dark in a 0.1 M sodium acetate solution using a potentiostat (HD Hokuto Denko HAB-151). The surface morphological variations and the structure of the deposited Cu_2O films were monitored using scanning electron microscopy (Zeiss Evols15) and X-ray diffractometry (Shimadzu (XD-D1)) with Cu-Kα ($\lambda = 1.5418$ Å) as the source of X-rays respectively. In order to compare the photocurrent spectral responses of the nano-cubic Cu_2O films with those of the microcrystalline Cu_2O films, photocurrent spectral response measurements of the Cu_2O film samples were made in a three electrode electrochemical cell containing a 0.1 M sodium acetate solution. The counter electrode and the reference electrode were a Pt sheet and the SCE respectively. The exposed area of the film to the electrolyte was ~4 mm^2 [1]. The photocurrent spectral response measurements were obtained using a phase sensitive detection method by chopping a monochromatic light beam at a chopping frequency of 60 Hz. The experimental setup consisted of a lock-in-amplifier (Stanford Research-SR 830 DSP), a potentiostat (Hokuto Denko HAB-151), a chopper (Stanford −SR 540), and a monochromator (Sciencetech-9010). In order to test LP gas sensing properties, the films were placed on a glass plate inside a cylindrical chamber made of aluminum having an internal diameter of 5 cm and a depth of 3 cm. Chamber was sealed using a cap made of Perspex. Gas sensing characteristics of micro-structured and nano-cubic Cu_2O films were investigated by measuring the resistance across the films using the two-point contact probe method. Electrical measurements were performed at different temperatures and measurements were acquired using a Keithly 2100 6 1/2 Digital Multimeter and a computer data logger. Silver contacts of ~1 mm in diameter were placed 1 cm apart on the film of area $1.5 \times 1\ cm^2$. The measurements were acquired for different LP gas concentrations having volume percentages of 2, 2.5, 3.5, and 5%, respectively by allowing a mixture of LP gas and dry air to flow into the gas sensing chamber while controlling the LP gas: dry air ratios using gas flow meters which were calibrated for the two gases. Care was taken to send the gas mixture through a column of silica gel which was freshly filled at each experiment. A total gas flow of 205 $cm^3\,min^{-1}$ was maintained throughout the experiment. The response of the films to LP gas was measured at temperatures 120, 150, 180, 200, and 230 °C.

3 Results and discussion Figure 1 shows the Mott–Schottky plots at each stage of the deposition of a nano-cubic Cu_2O film in comparison with the microcrystalline Cu_2O film. The Mott–Schottky plots shown in (Fig. 1) were obtained using Eq. (1) [29]:

$$\frac{1}{C^2} = \left(\frac{2}{e\varepsilon\varepsilon_0 N}\right)\left[V - V_{\mathrm{fb}} - \frac{k_{\mathrm{B}}T}{e}\right], \tag{1}$$

where C is the capacitance of the space charge region, ε_0 is the vacuum permittivity, ε is the dielectric constant of Cu_2O,

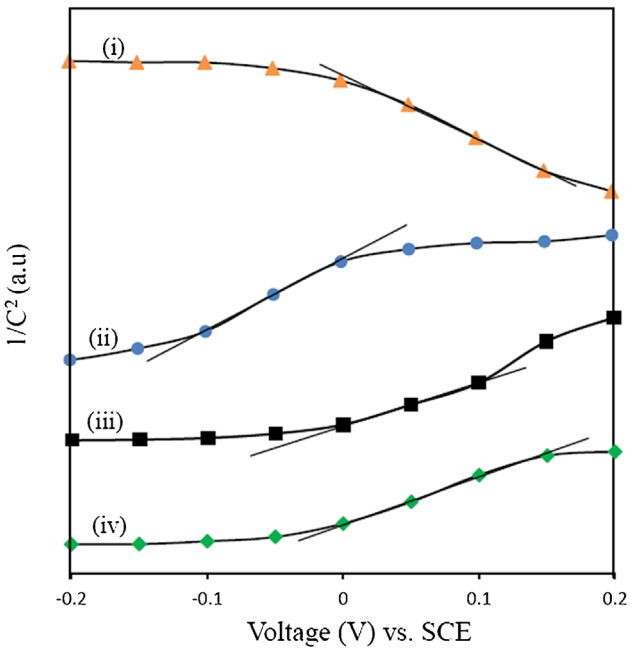

Figure 1 Mott–Schottky plots of the variation of capacitance of thin films against the applied voltage made in the dark in a 0.1 M sodium acetate solution at 10 kHz, (i) nano-cubic Cu_2O thin film as deposited on Ti substrate in the acetate bath of pH 7.6; (ii) nano-cubic Cu_2O thin film deposited on Ti substrate in an acetate bath of pH 7.6 and briefly annealed at 200 °C; (iii) nano-cubic Cu_2O thick film deposited using annealed film as a template; and (iv) microcrystalline Cu_2O thin film deposited on Ti substrate in an acetate bath of pH 6.0. Slope of the plots indicates the conductivity type of the films.

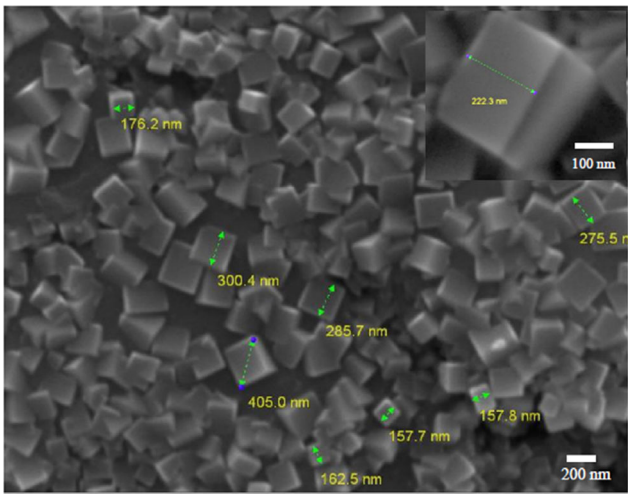

Figure 2 Scanning electron microscopic image of Cu_2O nano-cubes on Ti substrate fabricated in an acetate bath containing 0.1 M sodium acetate and 0.01 M cupric acetate of pH 7.6 at 60 °C for 30 min. The thickness of the nano-cubic thin film is ~500 nm. The inset shows an enlarged image of a single nano-cube (image was taken from a different Cu_2O nano-cubic template).

e is the electron charge, V is the applied potential, V_{fb} is the flat band potential of Cu_2O, k_B is the Boltzmann constant, T is the absolute temperature, and N is the acceptor/donor concentration [29]. According to the Mott–Schottky equation, a linear relationship of C^{-2} versus V can be observed. The Mott–Schottky plot shown in Fig. 1(i) corresponding to a nano-cubic thin Cu_2O film deposited at a pH of 7.6 gave a negative gradient indicating *p*-type conductivity. The plots in Fig. 1(ii) which corresponds to annealed nano-cubic thin Cu_2O film, Fig. 1(iii) which corresponds to the thick nano-cubic Cu_2O film deposited using the annealed thin film as a template, and Fig. 1(iv) which corresponds to a microcrystalline Cu_2O film all show positive gradients indicating that these films are of *n*-type conductivity.

Figure 2 shows a scanning electron microscopic (SEM) image of the surface morphology of a nano-cubic *p*-type Cu_2O thin film as deposited on Ti substrate in an acetate bath containing 0.1 M sodium acetate and 0.01 M cupric acetate at a pH of 7.6 for 30 min at 60 °C. It was found that the morphology of the electrodeposited films strongly depended on the pH value of the electrolyte. Figure 2 clearly shows Cu_2O nano-cubes having well defined edges with dimensions ranging from ~150–300 nm. These dimensions are much smaller compared to the dimensions (800 nm–1 μm) of shape controlled Cu_2O crystals obtained by Won et al. [4] using chemical bath deposition. Figure 3(a) shows a SEM image of the surface morphology of the nano-cubic *n*-type Cu_2O film fabricated using a thin Cu_2O nano-cubic template in comparison with the surface morphology of a microcrystalline *n*-type Cu_2O thin film (Fig.3(b)) fabricated on a Ti substrate in an acetate bath maintained at a pH of 6.0 without using a template. It is clear from (Fig. 3) that in (a) there is an agglomeration of a large number of nano-cubic crystals whereas in (b) grains have arbitrary shapes in the micro scale.

Figure 4 shows an X-ray diffraction pattern obtained for a nano-cubic Cu_2O film shown in Fig. 3(a) compared with standard data for Cu_2O (JCPDS: 05-0667). It is evident from these results that both the size and shape can be controlled using the fabrication method described earlier without disturbing the Cu_2O stoichiometry. In addition the Fig. 4 reveals that the nano-cubic Cu_2O thicker films are of single phase without any impurities. A comparison of the photocurrent spectral response patterns of the nano-cubic *n*-type Cu_2O film and its microcrystalline counterpart is shown in Fig. 5.

The observed positive photo current spectral response (*n*-type conductivity) agrees with the Mott–Schottky measurements. It also shows that the photo current spectral response peak of the template assisted nano-cubic *n*-type Cu_2O film is stronger compared to that of the *n*-type microcrystalline film despite both films have been deposited for the same time of 60 min. This is an indication that the nano-cubic *n*-type Cu_2O film fabricated using the template assisted method exhibits better light harvesting properties compared to the microcrystalline Cu_2O thin film due to the larger surface area produced by the increased number of

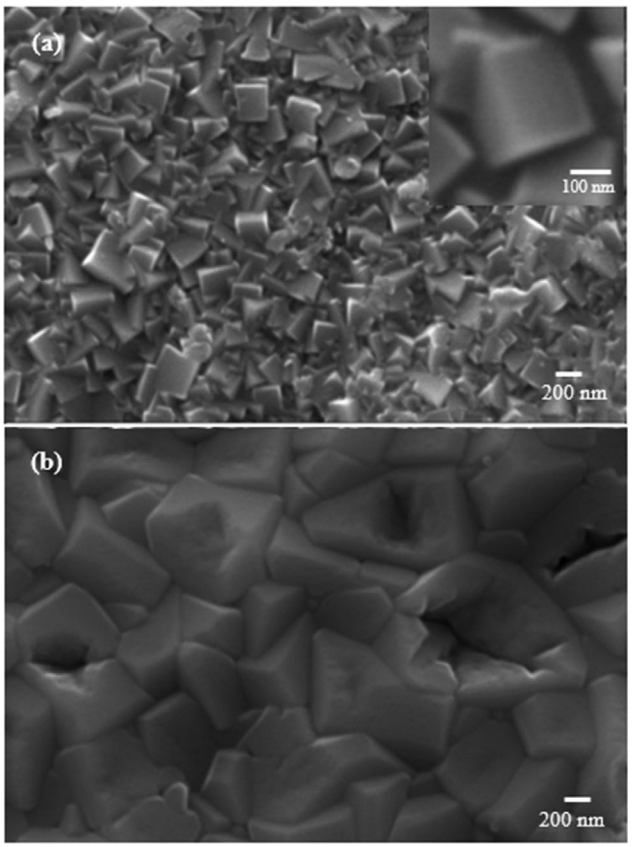

Figure 3 Scanning electron microscopic images of electrodeposited Cu_2O thin films deposited on Ti substrates at 60 °C (a) at pH 6.0 for 30 min after fabricating a *p*-type nano-cubic template at pH 7.6 for 30 min at 60 °C and annealing at 200 °C for 5 min (thickness of nano-cubic thicker film is ~2 μm) and (b) at pH 6.0 for 60 min without using a template (thickness of the microcrystalline thin film is ~2 μm). The inset in (a) shows an enlarged view of a nano-cube obtained from a different Cu_2O film prepared under the same conditions.

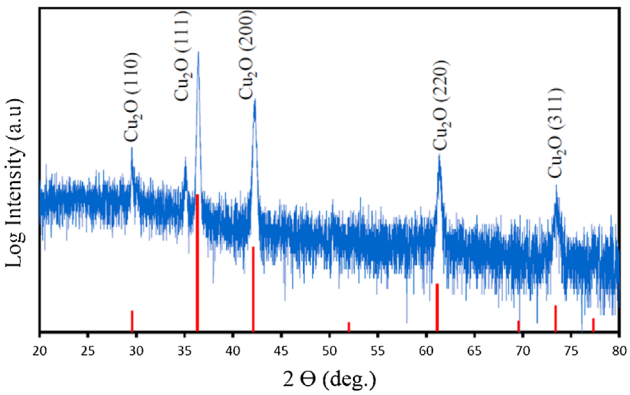

Figure 4 X-ray diffraction image of the nano-cubic *n*-type Cu_2O film deposited at pH 6.0 for 30 min after fabricating a *p*-type nano-cubic template at pH 7.6 for 30 min at 60 °C and annealing at 200 °C for 5 min in comparison with the standard data for Cu_2O (JCPDS: 05-0667).

grains at nano scale. It can also be seen that the photo current peak position of the nano-cubic *n*-type Cu_2O film has shifted slightly toward shorter wavelengths compared to that of the *n*-type microcrystalline film. This can be attributed to the dependence of the absorption of wavelength of Cu_2O films on the grain size at nano scale. For the calculation of the thicknesses of the Cu_2O thin films, the Faraday's Equation was used by assuming that only single phase Cu_2O was deposited and the density of the Cu_2O in the thin film form was equal to the bulk density which was 6000.0 kg m^{-3}. Ideally, the deposition thickness (d) follows Faraday's laws of electrolysis [30]:

$$d = \frac{MQ}{ne\rho AN_A}, \tag{2}$$

where M is the molecular weight of the deposit, Q is the total charge passed during deposition, n is the number of electrons taking part in the reduction, e is the charge of electron, N_A is the Avogadro's number, ρ is the bulk desity of the deposit (g cm^{-3}), and A is the area of the deposition (cm^2). Using Eq. (2) the thickness of the microcrystalline Cu_2O thin films deposited for 60 min under the applied potential −200 mV was estimated to be 2.0 μm [31, 32]. The thickness of the template was found to be 0.5 μm and at this thickness, the nano-cubes were not closely packed to provide a layer of uniform coverage. However, the total thickness of the nano-cubic thicker film deposited using the above template was found to be 1.9 μm (~2 μm). This film exhibited uniformly packed morphological structure and hence better gas sensing performance [19].

In order to evaluate the response of the *n*-type Cu_2O films when exposed to LP gas, measurements were carried out by varying the input gas concentration and the operating temperature of the sensor films as described in the experimental procedure. The response of the thin films to LP gas was determined using Eq. (3) [3]:

$$S = \frac{\Delta R}{R} = \frac{R_g - R_a}{R_a} \times 100\%, \; R_g > R_a, \tag{3}$$

where $\Delta R/R$ is the change of electrical dc-resistance, R_g is the resistance of the film in the presence of the gas-dry air mixture and R_a is the resistance of the film in the presence of dry air [3]. From the response measurements made for LP gas concentrations having volume percentages of 2, 2.5, 3.5, and 5%, at sensor operating temperatures of 120, 150, 180, 200, and 230 °C, respectively, the maximum response of thin films was observed at 180 °C at all concentrations. The temperature corresponding to the maximum response observed in this study is comparable to those reported by Jayatissa et al. [3] for *p*-type Cu_2O films exposed to Methane gas (180 °C) and by Shishiyanu et al. [18] for *p*-type Cu_2O thin films exposed to NO_2 gas (150 °C). Figure 6 shows the response variations of both microcrystalline and nano-cubic thin films at above operating temperatures for an input LP gas concentration of

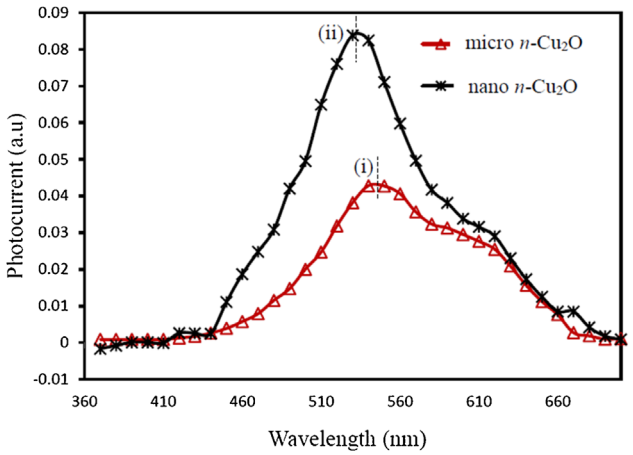

Figure 5 Photocurrent spectral response of (i) microcrystalline *n*-type Cu_2O thin film and (ii) template assisted nano-cubic *n*-type Cu_2O thicker film deposited in an acetate bath of pH 6.0.

2 vol.%. It can be seen from the Fig. 6 that the nano-cubic *n*-type Cu_2O film shows an approximately twofold increase in maximum response when compared to microcrystalline *n*-type Cu_2O film while the temperature corresponding to the maximum response remains unchanged.

It is obvious that, when the effective surface area is larger, the interactions between the adsorbed gases and metal oxide surface will be higher, leading to a higher response [33]. At lower temperatures, the response is restricted due to the slow rate of chemical reaction, and at high temperatures, it is restricted by the high rate of desorption. Therefore, the gas response reaches a maximum at some intermediate temperature. Results show that this maximum temperature is independent of the surface morphology. Figure 7 shows the temporal variation of gas response of both microcrystalline and nano-cubic *n*-type Cu_2O films for 2 vol.% LP gas at 180 °C. Both films showed good reproducibility for more than 20 LP gas ON/OFF cycles, which is an important characteristic for gas sensors. It can be seen from the figure that the microcrystalline *n*-type Cu_2O thin film has taken around 90 s to reach its steady state maximum value (response time). Compared to the microcrystalline film, the gradient of response versus time of nano-cubic *n*-type Cu_2O film is larger indicating that it reaches a higher response value faster. However, due to its larger surface area, the nano-cubic *n*-type Cu_2O film has taken a longer time to saturate its surface with LP gas molecules resulting in a response time of ~120 s. After reaching the steady state at stoppage of the LP gas, recovery time was about 90 s. In comparison with materials previously used for LP gas sensing, these films recorded very good recovery times and response times.

Figure 8 shows the gas response of *n*-type Cu_2O films as a function of LP gas concentration at 180 °C. According to the measurements shown in Fig. 8, the response increases with increasing LP gas concentration for both nano-cubic and microcrystalline *n*-type Cu_2O films. The response of a sensor depends on the removal of adsorbed oxygen from the sensing material surface. When the Cu_2O film is exposed to a small concentration of LP gas, the surface is covered only partially with adsorbed hydrocarbon molecules resulting in a small increase in resistance. With increasing concentration of LP gas, the surface coverage increases giving rise to an increased response. The mechanism of sensing by the Cu_2O films in this study can be interpreted as follows. When the films are exposed to atmosphere, adsorption of oxygen molecules in dry air causes a change in resistance of the film material [24]. At high temperatures, physisorbed H_2O is eliminated from the

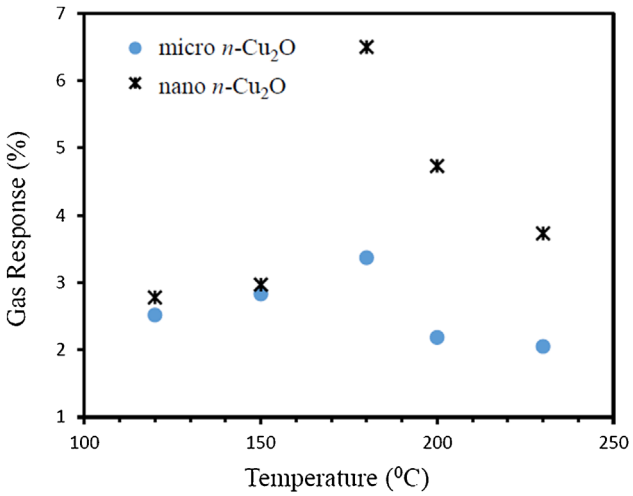

Figure 6 Variation of sensor response with different operating temperatures when exposed to 2 vol.% liquefied petroleum gas of microcrystalline (blue solid circles) and nano-cubic (crosses) *n*-type Cu_2O films fabricated on Ti substrates and nano-cubic template in an acetate bath at 60 °C, respectively.

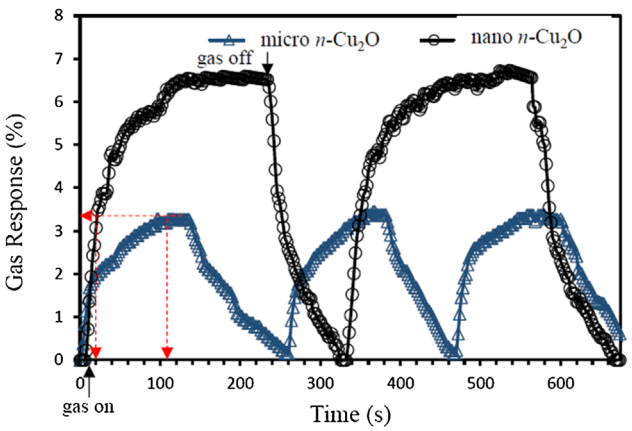

Figure 7 Variation of liquefied petroleum gas (2 vol.%) response with time at the temperature of 180 °C for ~2 μm thick microcrystalline (blue open triangles) and nano-cubic (black open circles) *n*-type Cu_2O films fabricated on Ti substrates and nano-cubic template in an acetate bath at 60 °C, respectively.

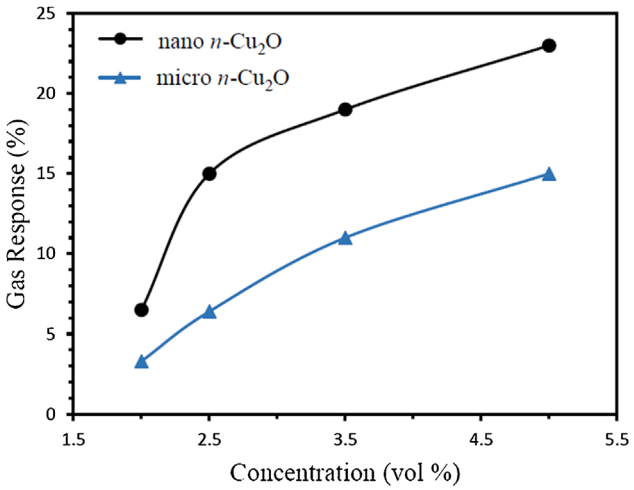

Figure 8 Variation of liquefied petroleum gas responses with different input concentrations of 2, 2.5, 3.5, and 5 vol.% for ~2 μm thick nano-cubic (black solid circles) and microcrystalline (blue solid triangles) n-type Cu_2O films at 180 °C, the temperature corresponding to the maximum response.

material surface and surface hydroxide groups are converted to oxygen species such as, O_2^-, O_2^{2-},O^-, and O^{2-}. The gas response originates due to the abstraction of hydrogen from hydrocarbons by the surface oxygen species. Despite the complexity of reactions, the sensing mechanism may be understood as follows [24, 26, 34–36]:

(I) Generation of surface oxygen species:

$$O_{2(gas)} \leftrightarrow O_{2(ads)}, \tag{4}$$

$$O_{2(ads)} + e^- \rightarrow O^-_{2(ads)}, \tag{5}$$

$$O^-_{2(ads)} + e^- \rightarrow 2O^-_{(ads)}\ . \tag{6}$$

(II) Reaction of hydrocarbon molecules with surface oxygen species:

$$C_nH_{2n+2} + O^-_{2(ads)} \leftrightarrow H_2O + C_nH_{2n}{:}O + e^-, \tag{7}$$

$$C_nH_{2n+2}{:}O + 2O^-_{(ads)} \leftrightarrow H_2O + C_nH_{2n}{:}O + 2e^-, \tag{8}$$

$$C_nH_{2n}{:}O + (3n-1)\ O^-_{(ads)} \leftrightarrow nCO_2 + nH_2O + (3n-1)\ e^-. \tag{9}$$

The overall reaction can be separated into two major steps, the generation of surface oxygen species (I) and the reaction of hydrocarbon molecules with suface oxygen species (II). While C_nH_{2n+2} represents hydrocarbon molecules, C_nH_{2n}:O represents partially oxydized intermediates on the Cu_2O surface. The actual reactions between hydrocarbons and surface oxygen species involve hydrocarbons and oxygenerated intermediates of various chain lengths [24, 26, 34]. As LP gas is admitted to the chamber, pressure on the film increases, causing the rate of adsorption to increase. Reaction of hydrocarbons with surface oxygen species causes the depletion of surface oxygen species and widening of the depletion layer. This increases the resistance of the film [24]. The observed variation in resistivity is similar to the results reported on detection of LP gas by Shukla [24] using SnO_2 thin films, by Yadav et al. [26] and Richa Srivastava [27] using ZnO nanostructures. Once the process reaches its equilibrium the stoppage of the LP gas flow causes the resistance to decrease back to its ambient value. Stability is an important factor for a gas sensor. The stability of the sensors was tested and after the initial few weeks (2 and 3 weeks), it was found that the sensor responses of both micro and nano-cubic sensors gradually reduced by ~10%. However, subsequent reponse measurements remained unchanged showing that the films were stable over longer timescales.

Table 1 shows a comparison of sensor responses of the microcrystalline and nano-cubic Cu_2O thin film sensors fabricated in this study to the results reported by other reserchers. The table lists performance indicators for materials used for LP gas sensing as well as instances when Cu_2O-based materials were used for sensing of other gases. As far as the LP gas sensing is concerned, eventhough the sensor response of the microcrystalline and nano-cubic Cu_2O films are relatively lower compared to the sensor responses exhibited by other materials, they show comparable or better response/recovery times. It is noted that the observed sensor responses of the films considered in this study occur at a moderate temperature (180 °C) compared to some of the highly responsive sensors which require the operating temperatures to be as high as 275–425 °C. It can also be seen that the sensor response of the nano-cubic Cu_2O film recorded in this study is twice as much compared to its microcrystalline counterpart. This can be attributed mainly to its increase in the effective surface area. The results reported in this study are also considered the first of their kind reported in literature for LP gas sensing using nano-cubic Cu_2O thin film structures.

4 Conclusion In summary, this study demonstrates the potential of Cu_2O, considered as an environmentally friendly (green) material, for sensing large organic molecules such as hydrocarbons that are constituents of LP gas. Study also shows that less sophisticated low-cost fabrication techniques

such as electrodeposition can be used to control the surface morphological properties of Cu_2O to obtain nano-cubic crystals having sizes of 150–300 nm without the use of toxic surfactants and commercially available relatively expensive templates. Our investigation revealed, that the nano-cubic Cu_2O thin films having the thickness of ~2 μm exhibits better gas response (6.5%) compared to the gas response (3.2%) of microcrystalline thin films having a similar thickness. This is a twofold increment at a relatively lower temperature of 180 °C. The nano-cubic sensor demonstrated a good response time (~120 s) and a recovery time (~90 s) which is the best recovery time reported for LP gas sensing. Gas response of both the *n*-type nano-cubic and microcrystalline Cu_2O films remained unchanged upon depreciation by ~10% initially (first 2 and 3 weeks). It is interesting to further investigate the effect of the cubic crystalline geometry on the sensor response. Further investigations warrant the testing of response to other gases which will also determine the sensor specificity of the material. Testing the material's potential to sense other important molecules in minute amounts is also of interest. The sensor response may also be further improved through doping, surface passivation, optimization of substrate and the ordering of nanostructures.

Acknowledgements Financial assistance from the research grant of University of Colombo, Sri Lanka (AP/3/2/2014/RG/08) is gratefully acknowledged. R. P. Wijesundara and K. D. R. N. Kalubowila of the Department of Physics, University of Kelaniya, Sri Lanka, are acknowledged for the assistance provided in making some of the experimental measurements.

References

[1] K. M. D. C. Jayathilaka, V. Kapaklis, W. Siripala, and J. K. D. S. Jayanetti, Semicond. Sci. Technol. **27**, 125019 (2012).
[2] X. Zou, H. Fan, Y. Tian, M. Zhang, and X. Yan, RSC Adv. **5**, 23401 (2015).
[3] A. H. Jayatissa, P. Samarasekara, and G. Kun, Phys. Status Solidi A **206**, 332–337 (2009).
[4] Y. H. Won and L. A. Stanciu, Sensors (Basel) **12**, 13019–13033 (2012).
[5] L. Wang, J. Fu, H. Hou, and Y. Song, Int. J. Electrochem. Sci. **7**, 12587–12600 (2012).
[6] X. Zou, H. Fan, Y. Tian, and S. Yan, Cryst. Eng. Commun. **16**, 1149 (2014).
[7] X. Zou, H. Fan, Y. Tian, M. Zhang, and X. Yan, Dalton Trans. **44**, 7811 (2015).
[8] W. Siripala, K. M. D. C. Jayathilaka, and J. K. D. S. Jayanetti, J. Bionanosci. **3**(2), 118–123 (2009).
[9] A. E. Rakshani, Solid State Electron. **29**, 7 (1986).
[10] Y. Zhai, H. Fan, Q. Li, and W. Yan, Appl. Surf. Sci. **258**, 3232–3236 (2012).
[11] C. Iida, M. Sato, M. Nakayama, and A. Sanada, Int. J. Electrochem. Sci. **6**, 4730–4736 (2011).
[12] P. E. de Jongh, D. Vanmaekelbergh, and J. J. Kelly, Chem. Mater. **11**, 3512–3517 (1999).
[13] J. A. Switr, C. J. Hung, L. Y. Huang, E. R. Switzer, D. R. Kammler, T. D. zeGolden, and E. W. Bohanan, J. Am. Chem. Soc. **120**, 3530 (1998).
[14] W. Siripala, L. D. R. D. Perera, K. T. L. De Silva, J. K. D. S. Jayanetti, and I. M. Dharmadasa, Sol. Energy Mater. Sol. Cells **44**, 251 (1996).
[15] W. J. Matthe, J. Siefried, and K. S. Choi, Adv. Mater. **16**, 1743 (2004).
[16] R. R. Salunkhe, V. R. Shinde, and C. D. Lokhande, Sens. Actuators B **133**, 296–301 (2008).
[17] Y. Tang, Z. Chen, Z. Jia, L. Zhang, and J. Li, J. Mater. Lett. **59**, 434–438 (2005).
[18] S. T. Shishiyanu, T. S. Shishiyanu, and O. I. Lupan, Sens. Actuators B **113**, 468–476 (2006).
[19] V. Cretu, V. Postica, A. K. Mishra, M. Hoppe, I. Tiginyanu, Y. K. Mishra, L. Chow, Nora H. de Leeuw, R. Adelung, and O. Lupan, J. Mater. Chem. A **4**, 6527 (2016).
[20] O. Lupan, V. Cretu, V. Postica, O. Polonskyi, N. Ababii, F. Schütt, V. Kaidas, F. Faupel, and R. Adelung, Sens. Actuators B **230**, 832–843 (2016).
[21] L.-J. Zhou, Y.-C. Zou, J. Zhao, P.-P. Wang, L.-L. Feng, L.-W. Sun, D.-J. Wang, and G.-D. Li, Sens. Actuators B **188**, 533–539 (2013).
[22] J. Zhang, J. Liu, Q. Peng, X. Wang, and Y. Li, Chem. Mater. **18**, 867–871 (2006).
[23] N. Bandara, C. Jayathilaka, D. Dissanayaka, and S. Jayanetti, J. Sens. Technol. **4**, 119–126 (2014).
[24] T. Shukla, J. Sens. Technol. **2**, 102–108 (2012).
[25] D. Haridas, A. Chowdhuri, K. Sreenivas, and V. Gupta, Int. J. Smart Sens. Intell. Syst. **2**, 3 (2009).
[26] B. C. Yadav, R. Srivastava, and A. Yadav, Sens. Mater. **21**, 87–94 (2009).
[27] R. Srivastava, Am. J. Eng. Res. (AJER) **3**, 174–179 (2013).
[28] A. M. More, J. L. Gunjakar, and C. D. Lokhande, Sens. Actuators B **129**, 671–677 (2008).
[29] N. F. Mott, Proc. R. Soc. Lond. A **171**, 27–38 (1939).
[30] R. P. Wijesundera, M. Hidaka, K. Koga, M. Sakai, and W. Siripala, Thin Solid Films **500**, 241–246 (2006).
[31] A. Paracchino, J. C. Brauer, J. E. Moser, E. Thimsen, and M. Graetzel, J. Phys. Chem. C **116**, 7341 (2012).
[32] K. M. D. C. Jayathilaka, A. M. R. Jayasinghe, G. U. Sumanasekara, V. Kapaklis, W. Siripala, and J. K. D. S. Jayanetti, Phys. Status Solidi B **252**, 1300–1305 (2015).
[33] V. R. Shinde, T. P. Gujar, C. D. Lokhande, R. S. Mane, and S.-H. Han, Sens. Actuators B **123**, 882–887 (2007).
[34] P. P. Sahay and R. K. Nath, Sens. Actuators B **133**, 222–227 (2008).
[35] S. Lenaerts, J. Roggen, and G. Maes, Spectrochim. Acta A **51**, 883–889 (1995).
[36] N. Yamazoe, J. Fuchigami, M. Kishikawa, and T. Seiyama, Proceedings the International Conference on Solid Films and Surfaces, Tokyo, Japan, 1978, Part A (Elsevier B.V, The Netherlands, 1979), pp. 335–344.

